# Candidacy Paper on TGC Determination at LEP2 Using the $q\bar{q}\tau\nu_\tau$ Channel

I. Bailey
University of Victoria

September 1, 1998

This paper reviews the theory of anomalous triple gauge boson couplings and their effects upon $W^+W^-$ production at LEP2 energies. The $q\bar{q}\tau\nu_\tau$ decay channel is studied in detail and analytical expressions for the differential cross-section are presented. The problem of reconstructing $q\bar{q}\tau\nu_\tau$ events is outlined and an improved method for recovering the tau's production angles from its decay products is introduced.

# Chapter 1

# Introduction

The Large Electron Positron (LEP) accelerator at CERN is now operating with beam energies greater than 80 GeV. Above this threshold it is kinematically possible to create pairs of real $W^{\pm}$ bosons[1] in the centre of mass frame. Experiments in this new energy regime are collectively referred to as **LEP2** to distinguish them from previous LEP research carried out with 45 GeV beams.

$W^+W^-$ pair production is of particular interest because the process involves a contribution from the coupling of three gauge bosons at a single vertex ($e^+e^- \rightarrow (Z^0, \gamma)_{virtual} \rightarrow W^+W^-$). The existence and form of these couplings are predicted by the standard model of particle physics: but they have not previously been well measured experimentally. This is because, until recently, only indirect, model-dependent measurements have been possible. LEP2 provides a unique opportunity for a more precise study [2].

It is expected from theoretical considerations [8], [11], [12] that *new physics* (beyond our current standard model) must operate in this *bosonic sector* at some, as yet unknown, energy scale. This motivates a rigorous search for deviations from the predicted triple gauge boson couplings (**TGC's**).

If present, anomalous couplings will alter the effective electromagnetic moments of the W bosons, the total number of W pairs produced, their angular distributions and those of their decay products. Just as measurements of the anomalous magnetic moments of the neutron and proton[3] led to the search for, and discovery of, nucleon substructure, so the measurement of the moments of the W boson may hint at new physics possibilities.

This paper focusses on the effects of anomalous TGC's on one possible decay channel of a W pair; that of $q\bar{q}\tau\nu_\tau$.

[1] $M_W \approx 80.33\ GeV$.

[2] To date, those direct measurements made at the Tevatron $p\bar{p}$ collider have placed relatively loose bounds on the couplings [4].

[3] Carried out by O. Stern in 1933.

Chapters 2.1 and 2.2 deal with the process of W pair production within and beyond the standard model respectively. The latter discussion introduces the concept of anomalous couplings and their physical origins. Chapter 2.3 presents the helicity formalism as a tool for studying the spin states of particles, which is then used to calculate the angular distributions and cross-sections for W pair production shown in Chapter 2.4. Chapter 3 is mainly concerned with the production of tau leptons from W decay and the dependence of the cross-section on the anomalous TGC's we would like to measure. Some details of the single pion decay mode of the tau are also given. The implications for further work in this area are summarised in Chapter 4.

# Chapter 2

# $W^+W^-$ Production

## 2.1 Standard Model

The standard model (SM) of particle physics partitions all observed, fundamental particles into one of three groups: leptons, quarks and gauge bosons.

Leptons are fermions (particles with half integral spin) which interact with other matter via the electromagnetic or *weak* [1] forces only. There are three generations of leptons, each consisting of one electrically charged and one electrically neutral fermion. The charged leptons are the electron, muon and tau(on) $(e, \mu, \tau)$. The neutral leptons are the associated neutrinos $(\nu_e, \nu_\mu, \nu_\tau)$. Their properties are summarised in tables 2.1 and 2.2.

| Lepton | Mass (MeV) | Mean Lifetime |
|---|---|---|
| $e^-$ | $0.51099907 \pm 0.00000015$ | $> 4.3 \times 10^{23} yr$ |
| $\mu^-$ | $105.658389 \pm 0.000034$ | $(2.19703 \pm 0.00004) \times 10^{-6} s$ |
| $\tau^-$ | $1777.05^{+0.29}_{-0.26}$ | $(290.0 \pm 1.2) \times 10^{-15} s$ |

Table 2.1: Properties of charged leptons.[2]

| Lepton | Mass (MeV) | (Mean Lifetime)/Mass |
|---|---|---|
| $\nu_e$ | – | $> 7 \times 10^9 s/eV$ (solar) |
| $\nu_\mu$ | $< 0.17 (90\% CL)$ | $> 15.4 s/eV (90\% CL)$ |
| $\nu_\tau$ | $< 18.2 (95\% CL)$ | – |

Table 2.2: Properties of neutral leptons.[2]

[1] The label 'weak' refers to the short-range nature of the interaction.

The second group of fermions in the SM experience the *strong* force in addition to the electroweak [2] force. Generically, particles which undergo strong interactions are referred to as hadrons. The fundamental (indivisible) hadrons are known as quarks. These, like the leptons, have three generations, where each generation contains a pair of quarks.

The standard model explains the forces exerted by one particle upon another as a consequence of the exchange of one or more gauge bosons ($\gamma, Z^0, W^+, W^-, g$). The gauge bosons propagate information about the electromagnetic ($\gamma, Z^0$), weak ($W^+, W^-, Z^0$) and strong (g) quantum numbers of a particle between points in space-time. The existence of gauge bosons arises naturally in the theory of the SM when we attempt to conserve the quantum numbers (i.e. electric charge, weak isospin and strong colour charge) of leptons and quarks in a Lorentz invariant way. This process is outlined in the next section for the case of the electroweak force.

Additionally, the SM contains the Higgs boson. Although this particle has not been observed to date its existence is assumed where necessary in the remainder of this paper.

### 2.1.1 TGC Lagrangian

The dynamics of any quantum mechanical system can be described by a Lagrangian [3] (or equivalently Hamiltonian) containing contributions from all of the interacting fields. Physical particles are then interpreted as quantised excitations of the fields. Mathematically, each field is represented by a potential function or, more generally, a potential operator. In relativistic quantum mechanics the Lagrangian is required to be Lorentz invariant[4] , which is achieved by writing all of the potentials in the form of four vectors (so that particle 'X' enters the Lagrangian as a four-vector potential '$X^\mu$').

However, if an experiment is carried out at some characteristic energy, E, the existence of particles with masses, $m_i$ , where $m_i \gg E$ may not be discernible [5] In this case, there is an effective Lagrangian which describes the observed low-energy behaviour but does not contain any explicit references to the high mass particles (i.e. the potentials associated with the high mass particles are absent from the effective Lagrangian). This is often referred to as *integrating out* (or *integrating in*) the high energy degrees of freedom.

The Lagrangian originally used by Fermi to describe weak decays is one such effective low-energy approximation. Fermi made the physical assumption that the range of the weak interaction was small enough to be neglected. In this case, all four of the fermions which take part in a weak decay must meet at a single point. However, this model is deficient

[2] The electromagnetic and weak interactions are understood as being parts of a single unified 'electroweak' interaction.

[3] This paper uses the Lagrangian, $L$, and the Lagrangian density, $\mathcal{L}$, interchangeably. In general $L = \int \mathcal{L}\, d^3x$.

[4] More properly, it is the *action*, $S$, which is required to be Lorentz invariant, $S = \int L \cdot dt$.

[5] Particles which are *confined* by an interaction potential such that they only propagate over characteristic distances, $\lambda$, where $E \ll \frac{1}{\lambda}$ will also remain unobserved. E.g. quarks in a proton.

as it does not allow either the initial or final states to have orbital angular momenta. As a consequence, the contribution of the lowest order partial wave to the cross-section [6] for the scattering of electrons, $e^-$, from electron neutrinos, $\nu_e$, diverges unphysically (violating *unitarity* [7]).

To remove the divergence it is necessary to hypothesise the existence of the W boson to mediate the weak decay [8]. The creation of an intermediate W boson state is favoured when the centre of mass energy of a reaction is close to the W mass, $m_w$. At energies far above $m_w$ the cross-section falls asymptotically to zero in an analogous fashion to the response of a harmonic oscillator being driven above its resonant frequency.

In the SM, the $W^+$ and $W^-$ bosons only mix leptons of the same generation. A charged lepton and its associated neutrino can then be thought of as a two-fold degenerate eigenstate of the weak interaction. Further weak eigenstate doublets can be formed from linear combinations of the quark mass eigenstates by a unitary transformation. It is therefore convenient when considering electroweak processes to write a lepton or quark generation as a two dimensional column vector.

The vector is a representation of the generation in *weak isospin space*. The upper component is conventionally assigned a weak isospin value of $+1/2$ and the lower component a value of -1/2. In this abstract space the W boson is a rotation operator which transforms an isospin $+1/2$ object into a -1/2 object and vice versa. The process is mathematically similar to the *flipping* of an electron's spin through its interaction with a single photon.

Since two operators are not sufficient to describe a general rotation in a two dimensional complex space, a third gauge boson, $W^0$ or $W_3$, is introduced in analogy with the three Pauli spin matrices needed to generate the rotations of spin $\frac{1}{2}$ objects in physical space. The introduction of the third boson is also crucial in preventing further high-energy divergences, as can be seen explicitly in section 2.3.

If weak isospin is a conserved quantum number then physics (and hence the Lagrangian) must be invariant under rotations in weak isospin space. This constraint is equivalent to imposing $SU(2)$ gauge invariance on the Lagrangian. This is in addition to the $U(1)$ gauge invariance which the Lagrangian must exhibit in order to conserve electric charge.

Equation 2.1 shows a simplified[9] Lagrangian for a lepton doublet, $\Psi$, interacting with the three weak gauge boson fields, $\vec{W}_\mu$. The $\gamma^\mu$ are the Dirac matrices [10]. The components of $\vec{\tau}$ are the Pauli spin matrices. $\bar{\Psi}$ is defined as $\Psi^\dagger\gamma^0$, where $\dagger$ denotes the Hermitean conjugate.

[6] The cross-section is defined as the modulus squared of the scattering amplitude integrated over all angles. This gives the effective area of the incident beams which react to form the specified decay products.

[7] Unitarity is the requirement that a probability cannot exceed one.

[8] The first direct experimental evidence for the existence of the W boson was reported by UA1,UA2 1983.

[9] The V-A nature of the coupling has been ignored.

[10] Unless otherwise stated, formulas in this paper use the standard convention that Greek indices $(\mu, \nu, ...)$ run from one to four and Roman indices $(i, j, ...)$ run from one to three.

$$\mathcal{L} \propto \bar{\Psi}\gamma^{\mu}\vec{W}_{\mu}\cdot\vec{\tau}\,\Psi \tag{2.1}$$

Applying $SU(2)$ gauge invariance to equation 2.1 then generates an extra term which represents self-interactions between the bosons. This is shown in equation 2.2. Terms which represent interactions between four gauge bosons at a single vertex have been suppressed. The third weak gauge boson, $W_3$, has been replaced with a linear admixture of the physically observable $Z^0$ boson and photon, whilst $W_1$ and $W_2$ have been re-expressed in terms of $W^+$ and $W^-$. $A_\mu$ is the usual electromagnetic four-vector potential used in classical electrodynamics. The expression for $W_3$ defines the *weak mixing angle*, $\theta_w$. For completeness, the relationship between the primordial electromagnetic field $B$ and the observable $Z^0$ and photon is also shown.

$$\begin{aligned}
\mathcal{L}_{SM}^{TGC} &\propto \epsilon_{ijk}\left(\partial^{\mu}W_j^{\nu} - \partial^{\nu}W_j^{\mu}\right)W_k^{\mu}W_l^{\nu} \\
&\propto \left[W^{-\mu\nu}W_{\nu}^{+} - W^{+\mu\nu}W^{-\nu}\right](\sin\theta_w A_{\mu} + \cos\theta_w Z_{\mu}) \\
&+ \left[A^{\mu\nu}\sin\theta_w + Z^{\mu\nu}\cos\theta_w\right]W_{\mu}^{+}W_{\nu}^{-}
\end{aligned} \tag{2.2}$$

$$\begin{aligned}
W^{\mu\nu} &= \partial^{\mu}W^{\nu} - \partial^{\nu}W^{\mu} \\
W_3^{\mu} &= \cos\theta_w Z^{\mu} + \sin\theta_w A^{\mu} \\
(B^{\mu} &= -\sin\theta_w Z^{\mu} + \cos\theta_w A^{\mu}) \\
W^{\pm} &= \frac{1}{\sqrt{2}}(W_1 \mp \imath W_2)
\end{aligned}$$

Equation 2.2 is the SM Lagrangian for triple gauge boson interactions where the constant of proportionality is $\frac{e}{\sin\theta_w}$.

### 2.1.2 Feynman Diagrams

Provided that the coupling between particles can be treated as small, a Lagrangian can be Fourier transformed to momentum space and expanded as a perturbation series in terms of the coupling constants. Each term in the series can be associated with a *Feynman diagram* which provides a topological, classical interpretation for what is actually a quantum mechanical event. The contribution to the $e^+e^- \to W^+W^-$ process from the TGC interaction of equation 2.2 can be represented at first order by figures 2.1 a, b.

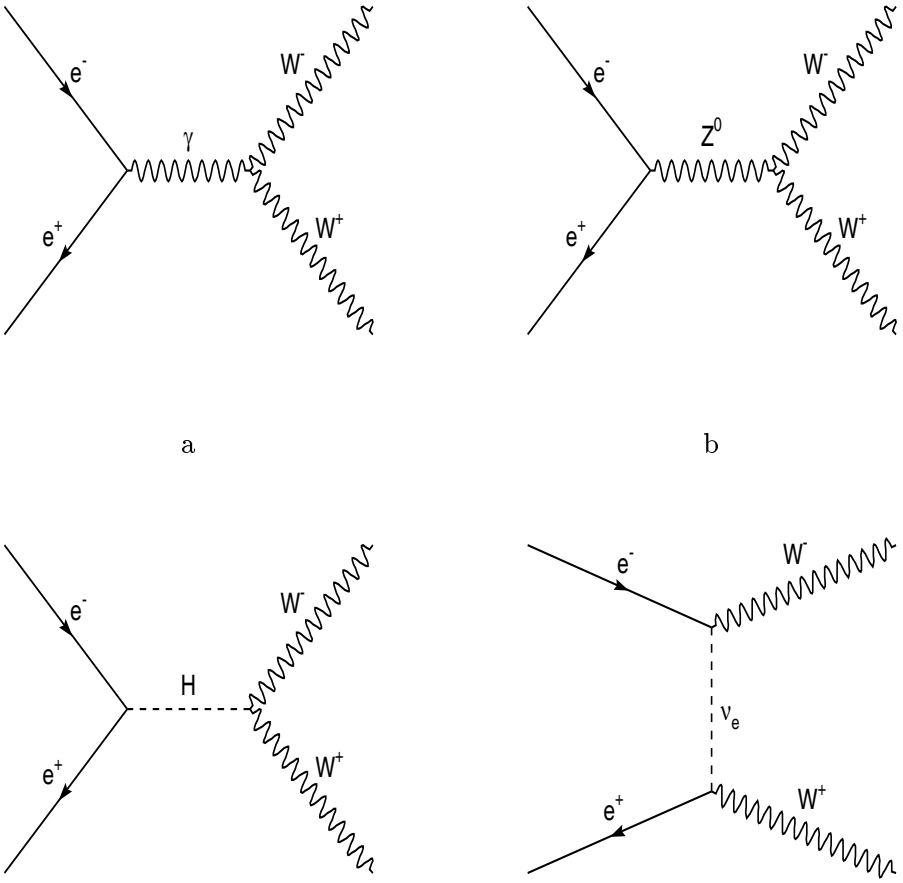


Figure 2.1: Tree-level Feynman diagrams showing $W^+W^-$ production from the annihilation of an electron and positron. Diagrams (a) and (b) contain the triple gauge boson couplings $\gamma W^+W^-$ and $Z^0W^+W^-$ respectively. Diagram (c) shows the same topology as in (a) and (b) but evolves through an intermediate Higgs boson state and gives a negligible contribution to the reaction at LEP2 energies (see main text). Diagram (d) shows the electron and positron scattering through the exchange of a neutrino. This last diagram is completely independent of the triple gauge boson couplings.

Feynman diagrams which correspond to first order terms in a perturbation expansion are generically referred to as *tree-level*, whilst the specific topology shown is known as s-channel. The $W^+W^-$ final state can also be attributed to the exchange of a neutrino in the t-channel configuration shown in figure 2.1 d.

In this paper the mass of the electron, $m_e$, is taken to be zero, as it is many orders of magnitude smaller than the LEP beam energies. However, in a full analysis the introduction of a finite electron mass requires a coupling to the Higgs boson. For completeness this diagram is shown in 2.1 c.

In reality it is not possible to specify which Feynman diagram led to the creation of a particular $W^+W^-$ pair in a particle detector. As the system is quantum mechanical it evolves through all possible diagrams simultaneously. This is shown in equation 2.3 of the next section, where the total scattering amplitude is given by the coherent sum of the individual contributions.

### 2.1.3 Scattering Amplitudes

The matrix elements (scattering amplitudes) which give the probability of a given initial state evolving to a given final state in quantum mechanics are found from the perturbative expansion of the Lagrangian using the Feynman rules. The transition rate (and hence the reaction cross-section) can then be found from Fermi's Golden Rule.

The Lorentz invariant scattering amplitudes for the first-order processes shown in figures 2.1 a,b,d are given in equations 2.4, 2.5 and 2.6 in terms of the $e^-$ and $e^+$ spinors[11] (denoted $u$ and $v$), and the $W^-$ and $W^+$ boson polarisation vectors (denoted $\epsilon_-$ and $\epsilon_+$). $g_{\mu\nu}$ is the Minkowski metric tensor and $k, \bar{k}, q$ and $\bar{q}$ are the four-momenta of the $e^-, e^+, W^-$ and $W^+$ respectively.

$$M_{TGC} = M_\gamma + M_Z + M_\nu \tag{2.3}$$

$$\begin{aligned} M_\gamma &= -e^2 \{\bar{v}\gamma_\mu u\} \left[\frac{g^{\mu\nu}}{s}\right] \\ &\quad \left\{\epsilon_+^{*\alpha}(g_{\alpha\beta}(\bar{q}-q)_\nu - g_{\alpha\nu}(q+2\bar{q})_\beta + g_{\beta\nu}(2q+\bar{q})_\alpha)\epsilon_-^{*\beta}\right\} \end{aligned} \tag{2.4}$$

$$\begin{aligned} M_Z &= -e^2 \left\{\bar{v}\gamma_\mu(1 - \frac{1-\gamma^5}{4\sin^2\theta_w})u\right\} \left[\frac{g^{\mu\nu} - (\bar{k}+k)^\mu(\bar{k}+k)^\nu/m_Z^2}{s - m_Z^2}\right] \\ &\quad \left\{\epsilon_+^{*\alpha}(g_{\alpha\beta}(\bar{q}-q)_\nu - g_{\alpha\nu}(q+2\bar{q})_\beta + g_{\beta\nu}(2q+\bar{q})_\alpha)\epsilon_-^{*\beta}\right\} \end{aligned} \tag{2.5}$$

[11] In relativistic quantum mechanics, the wavefunction for a fermion is not a solution of the time-dependent Schrödinger equation but of the (Lorentz-invariant) Dirac equation. The eigenstates of the Dirac equation are referred to as *spinors*.

$$M_\nu = -\frac{e^2}{8\sin^2\theta_w}\left\{\bar{v}\epsilon_+^{*\alpha}\gamma_\alpha(1-\gamma^5)\right\}\left[\frac{\gamma_\mu(\bar{k}-\bar{q})^\mu}{(\bar{k}-\bar{q})^2}\right]\left\{\epsilon_-^{*\beta}\gamma_\beta(1-\gamma_5)u\right\} \quad (2.6)$$

Explicit formulae for the scattering amplitudes in terms of observable quantities are developed using the helicity formalism in section 2.3.

## 2.2 Anomalous Couplings

### 2.2.1 Phenomenological Lagrangian

It was first shown by Hagiwara et al [13] (following from the work of Gaemers and Gounaris [16]) that the most general description of the coupling between three vector bosons (ignoring any theoretical or experimental constraints) requires a Lagrangian with seven operators. Higher order operators can be decomposed into linear combinations of these seven, which thus form a basis set.

The phenomenological Lagrangian is shown below, subdivided into the terms 2.7- 2.13. V is the four-vector potential of either a $Z^0$ boson or a photon, $\gamma$. In the latter case, $V^\mu$ can be written as $A^\mu$ for consistency with classical electrodynamics. $\epsilon_{\mu\nu\rho\sigma}$ is the 'totally antisymmetric' or 'Bjorken-Drell' symbol, defined such that $\epsilon^{0123} = \epsilon_{0123} = 1$.

$$\imath\mathcal{L}_{eff}^{WWV}/g_{WWV} = g_1^V V^\mu(W^-_{\mu\nu}W^{+\nu} - W^+_{\mu\nu}W^{-\nu}) \quad (2.7)$$

$$+ \kappa_V W^+_\mu W^-_\nu V^{\mu\nu} \quad (2.8)$$

$$+ \frac{\lambda_V}{m_W^2}V^{\mu\nu}W^{+\rho}_\nu W^-_{\rho\mu} \quad (2.9)$$

$$+ \imath g_5^V \epsilon_{\mu\nu\rho\sigma}((\partial^\rho W^{-\mu})W^{+\nu} - W^{-\mu}(\partial^\rho W^{+\nu}))V^\sigma \quad (2.10)$$

$$+ \imath g_4^V W^-_\mu W^+_\nu(\partial^\mu V^\nu + \partial^\nu V^\mu) \quad (2.11)$$

$$- \frac{\tilde{\kappa}_V}{2}W^-_\mu W^+_\nu \epsilon^{\mu\nu\rho\sigma}V_{\rho\sigma} \quad (2.12)$$

$$- \frac{\tilde{\lambda}_V}{2m_W^2}W^-_{\rho\mu}W^{+\mu}_\nu \epsilon^{\nu\rho\alpha\beta}V_{\alpha\beta} \quad (2.13)$$

$$W_{\mu\nu} = \partial_\mu W_\nu - \partial_\nu W_\mu$$

The standard model Lagrangian is recovered by setting $\kappa_\gamma, \kappa_Z, g_1^\gamma, g_1^Z$ to one and all other parameters to zero.

In the phenomenological approach, the *coupling constants* $(g_1, \kappa, \lambda, g_4, g_5, \tilde{\kappa}, \tilde{\lambda})$ are free parameters to be fitted to the data.

The terms of the phenomenological Lagrangian can be classified according to their symmetry properties under parity [12] , $\mathcal{P}$, and charge conjugation [13] , $\mathcal{C}$ transformations. [9]. This information is summarised in table 2.3.

| Parameter | Violates | | |
|---|---|---|---|
| | C | P | CP |
| $g_1$ | | | |
| $\kappa$ | | | |
| $\lambda$ | | | |
| $g_5$ | • | • | |
| $g_4$ | | • | • |
| $\tilde{\kappa}$ | • | | • |
| $\tilde{\lambda}$ | | | • |

Table 2.3: Summary of the symmetry properties of the terms in the phenomenological Lagrangian under charge conjugation and parity .

It is usual to discard those $\gamma WW$ terms which violate $\mathcal{CP}$ symmetry as their values are heavily constrained by the results of previous experiments. Moreover, the value of $g_1^\gamma$ is fixed to one. This leaves a total of nine independent parameters to describe the combined $\gamma WW$ / $ZWW$ vertex.

The $\mathcal{CP}$ conserving $\gamma WW$ couplings can be associated with a classical multipole expansion of the W boson. Equations 2.14, 2.15 and 2.16 show the electric charge, the magnetic dipole moment and the electric quadrupole moment of the W.

$$q_w = e g_1^\gamma \tag{2.14}$$

$$\mu_w = \frac{e}{2m_w}(1 + \kappa_\gamma + \lambda_\gamma) \tag{2.15}$$

$$Q_w = -\frac{e}{m_w^2}(\kappa_\gamma - \lambda_\gamma) \tag{2.16}$$

[12] A parity transformation is the inversion of the spatial co-ordinate system. E.g. in Cartesian co-ordinates $x \mapsto -x$, $y \mapsto -y$ and $z \mapsto -z$.

[13] A charge conjugation transformation is the replacement of each particle in a Lagrangian with its associated anti-particle. E.g. $W^+ \mapsto W^-$ and $W^- \mapsto W^+$.

All standard model vertices have an energy dimension of four[14], i.e. they can be written with units of $eV^4$. Such vertices are renormalisable (do not give divergences at high energies) and occur naturally in gauge symmetric theories. In the phenomenological TGC Lagrangian all terms are of dimension four except for the two *quadrupole* terms, $\lambda_V, \tilde{\lambda_V}$, which are of dimension six.

### 2.2.2 Theoretical Origins of Anomalous Couplings

It is advantageous to reduce the number of free parameters in the phenomenological Lagrangian to simplify the procedure of determining the parameters from the data. It has been shown [3] that it is insufficient to impose gauge symmetry, as all of the terms (2.7-2.13) can be made $SU(2) \otimes U(1)$ gauge invariant (and hence renormalisable) with the addition of extra terms of higher dimension.

An alternative method, introduced by Buchmuller and Wyler [14], is to construct all possible $SU(2) \otimes U(1)$ gauge invariant operators from the SM fields. An effective low-energy Lagrangian is then constructed using only those operators of dimension 6 or lower. This approach is based on the premise that *new physics* occurs at some energy scale, $\Lambda_{NP}$, far above $m_W$. In this case, higher dimensional contributions to the Lagrangian are suppressed by a factor of $1/\Lambda_{NP}$ and can be ignored.

In most contemporary papers (eg [5],[14],[15]) the mass of the Higgs boson, $m_H$, is taken to be small compared to $\Lambda_{NP}$. This assumption leaves three terms (shown in equation 2.17) which generate anomalous triple gauge boson couplings[15] but are relatively unconstrained by current measurements[5]. $\Phi$ is the Higgs doublet[16] , which can be replaced by its vacuum expectation value in order to compare equations 2.17 and 2.7.

$$\begin{aligned}
\mathcal{L}_{NP,TGC} &= \imath \frac{g\alpha_{W\phi}}{m_W^2}(D_\mu \Phi)^\dagger \vec{\tau} \cdot \hat{\vec{W}}^{\mu\nu}(D_\nu \Phi) \\
&+ \imath \frac{g'\alpha_{B\phi}}{m_W^2}(D_\mu \Phi)^\dagger B^{\mu\nu}(D_\nu \Phi) \\
&+ \frac{g\alpha_W}{6m_W^2}\vec{\hat{W}}_\nu^\mu(\vec{\hat{W}}_\rho^\nu \times \vec{\hat{W}}_\mu^\rho) \qquad (2.17)
\end{aligned}$$

$$\hat{W}_{\mu\nu}^{(i)} = \partial_\mu W_\nu^{(i)} - \partial_\nu W_\mu^{(i)} - g\epsilon^{ijk} W_\mu^{(j)} W_\nu^{(k)}$$

[14] In *natural units* ($\hbar = c = 1$) all other units are reduced to some power of the unit of energy.

[15] Higher order couplings are also generated.

[16] The Higgs doublet is a two dimensional column vector in weak isospin space, one component of which is conventionally set to zero by a redefinition of the co-ordinate system in a process known as 'spontaneous symmetry breaking'.

$$
\begin{aligned}
B_{\mu\nu} &= \partial_\mu B_\nu - \partial_\nu B_\mu \\
D_\mu \Phi &= \partial_\mu \Phi + \imath \frac{g}{2} \vec{\tau} \cdot \vec{W}_\mu \Phi - \imath \frac{g}{2} \tau_3 B_\mu \Phi
\end{aligned}
$$

The relation between the coefficients $\alpha_W$, $\alpha_{W\phi}$ and $\alpha_{B\phi}$ and those of the previous section are shown below.

$$
\begin{aligned}
\alpha_W &= \lambda_\gamma && (2.18) \\
&= \lambda_Z \\
\alpha_{W\phi} &= \sin^2\theta_w \kappa_\gamma + \cos^2\theta_w \kappa_Z - 1 && (2.19) \\
\alpha_{B\phi} &= \cot^2\theta_w (\cos^2\theta_w g_1^Z - \kappa_Z + \sin^2\theta_w) && (2.20)
\end{aligned}
$$

where

$$
\cos^2\theta_w \cdot (g_1^Z - \kappa_Z) = \sin^2\theta_w \cdot (\kappa_\gamma - 1) \qquad (2.21)
$$

Contributions to $\alpha_W$ would be generated by either a boson or fermion field operating at the new physics scale[5]. More complicated interactions would be needed to generate $\alpha_{W\phi}$ and $\alpha_{B\phi}$.

If the Higgs boson does not exist or else has a mass comparable to $\Lambda_{NP}$ then different terms are induced, whose largest effects will be upon the coupling of the longitudinally[17] polarised gauge bosons [12].

If the new physics energy scale is not large with respect to $m_w$ then higher dimension operators can no longer be ignored. This would be the case if, for example, there exists a $Z'$ boson of a mass comparable with the $Z^0$[10].

## 2.3 Helicity Formalism

The helicity formalism[17] is a useful convention for analysing the spin states of particles in a reaction. Rather than expressing the spin vectors with respect to a fixed frame of reference, the helicity of a particle is given by the projection of its spin, $\vec{s}$, onto its direction of motion, $\vec{p}$ (equation 2.22).

$$
h = \frac{\vec{s} \cdot \vec{p}}{|\vec{p}|} \qquad (2.22)
$$

[17] Longitudinal polarisation is equivalent to the requirement that the spin vector of a particle is orthogonal to its direction of motion.

This is particularly pertinent in the case of the decay of a W boson to two fermions, as the fermions are produced in fixed *chiral states* [18].

The scattering amplitude for a final state of definite helicity is known as a helicity amplitude. Equations 2.23, 2.24 and 2.25 show the helicity amplitudes for the production of on-shell [19] $W^+W^-$ bosons derived for the tree-level Feynman diagrams in figure 2.1.

The amplitudes depend only on the variables $\theta$, $\lambda_1$, $\lambda_2$, $\sigma_1$, $\sigma_2$, $\gamma$, $\beta$, the SM parameter $\theta_w$ and the masses of the particles involved. $\theta$ is the $W^-$ production angle with respect to the incident $e^-$ beam direction. $\lambda_1, \lambda_2, \sigma_1$ and $\sigma_2$ are the helicities of the $W^-, W^+, e^-$ and $e^+$ respectively. $\gamma$ is the Lorentz factor for either the $W^-$ or $W^+$ ($\gamma = E_{W^-}/m_{W^-} = E_{W^+}/m_{W^+}$) and $\beta$ is the associated velocity in units of c. $\theta_w$ is the weak mixing angle introduced in equation 2.2.

$$M = M_\gamma + M_Z + M_\nu$$

$$\begin{aligned}
M_\gamma &= \frac{-e^2\beta}{2}\frac{1}{\sqrt{1+\lambda_1^2}}\frac{1}{\sqrt{1+\lambda_2^2}} \\
&\Bigg\{ (1-\sigma_1\sigma_2)\Big[ (\lambda_1\lambda_2(1+\lambda_1\lambda_2) - (2\gamma^2+1)(\lambda_1^2-1)(\lambda_2^2-1))\sin\theta \\
&+ 2\gamma(\lambda_1(1-\lambda_2^2)+\lambda_2(1-\lambda_1^2))\cos\theta \Big] \\
&+ (\sigma_1-\sigma_2)(\lambda_1^2-\lambda_2^2) \Bigg\}
\end{aligned} \tag{2.23}$$

$$\begin{aligned}
M_Z &= \frac{e^2\beta}{8\sin^2\theta_w}\frac{m_w^2\gamma^2}{m_w^2\gamma^2 - m_z^2}\frac{1}{\sqrt{1+\lambda_2^2}}\frac{1}{\sqrt{1+\lambda_1^2}} \\
&\Bigg\{ (1-\sigma_1\sigma_2)\Big[ (4\sin^2\theta_w - 1) \\
&( (\lambda_1\lambda_2(1+\lambda_1\lambda_2) - (2\gamma^2+1)(\lambda_1^2-1)(\lambda_2^2-1))\sin\theta \\
&+ 2\gamma(\lambda_1(1-\lambda_2^2)+\lambda_2(1-\lambda_1^2))) \\
&+ 2\gamma(\lambda_1^2-\lambda_2^2) \Big] \\
&+ (\sigma_1-\sigma_2)\Big[ (4\sin^2\theta_w - 1)2\gamma(\lambda_1^2-\lambda_2^2)
\end{aligned}$$

[18] Chiral states and helicity states are equivalent for particles with a large Lorentz factor, $\gamma$.

[19] 'On-shell' particles obey the relativistic energy equation, $m^2 = E^2 - p^2$. Particles which do not obey this equality are known as 'virtual' and cannot propagate in free space.

$$
\begin{aligned}
&+ \quad (\lambda_1\lambda_2(1+\lambda_1\lambda_2) - (2\gamma^2+1)(\lambda_1^2-1)(\lambda_2^2-1))\sin\theta \\
&+ \quad 2\gamma(\lambda_1(1-\lambda_2^2)+\lambda_2(1-\lambda_1^2)) \quad \Big] \quad \Bigg\} \qquad (2.24)
\end{aligned}
$$

$$
\begin{aligned}
M_\nu \quad = \quad & \frac{e^2(1+\sigma_2)(1-\sigma_1)}{4\beta\sin^2\theta_w}\frac{1}{\sqrt{1+\lambda_1^2}}\frac{1}{\sqrt{1+\lambda_2^2}} \\
\Bigg\{ \quad & (\lambda_1^2-1)(\lambda_2^2-1)\left(\frac{1}{\gamma^2(1+\beta^2-2\beta\cos\theta)}-\gamma^2\right)\sin\theta \\
+ \quad & \lambda_1^2\lambda_2^2\left(\frac{\beta^2+\beta(\lambda_2-\lambda_1)-\lambda_1\lambda_2}{1+\beta^2-2\beta\cos\theta}+\lambda_1\lambda_2\right)\sin\theta \\
+ \quad & (\lambda_1^2-1)\lambda_2\left(\frac{1-\lambda_2\beta}{\gamma(1+\beta^2-2\beta\cos\theta)}-\gamma\right)(\cos\theta+\lambda_2) \\
+ \quad & (\lambda_2^2-1)\lambda_1\left(\frac{1+\lambda_1\beta}{\gamma(1+\beta^2-2\beta\cos\theta)}-\gamma\right)(\cos\theta-\lambda_1) \quad \Bigg\} \qquad (2.25)
\end{aligned}
$$

The $W$ bosons have a spin of one and hence $\lambda_1$ and $\lambda_2$ may take the values $+1, 0, -1$. (The positive and negative helicity states correspond to transverse polarisations and the zero helicity state corresponds to longitudinal polarisation.) The electron and positron are fermions with a spin of one half: but, in order to simplify the algebra, $\sigma_1$ and $\sigma_2$ have been defined to take the values $\pm 1$ rather than $\pm\frac{1}{2}$.

With these conventions the amplitudes are all zero unless $\mid \sigma_1 - \sigma_2 \mid$ is equal to two, which corresponds to there being one unit of angular momentum either parallel or anti-parallel to the $e^-$ beam direction. This constraint is present in both the s-channel and t-channel but arises through two different mechanisms.

The s-channel contributions, $M_\gamma$ and $M_Z$, are constrained because they evolve through an intermediate gauge boson (a photon and a $Z^0$ respectively) which itself has a spin of one [20]. However, the t-channel, $M_\nu$, is constrained not by its topology but by the nature of the W boson coupling to fermions [21]. Moreover, the couplings further restrict the t-channel to only give a contribution in the anti-parallel case mentioned above. It is also worth noting that the $Z^0$ part of the s-channel shows a less severe form of this asymmetry, as it has larger couplings in the anti-parallel case than in the parallel case. This is a comparatively small, although important, effect at LEP2 energies.

The high energy limit corresponds to: $s \to \infty$, $\beta \to 1$, $\gamma \to \infty$. Applying these transformations to the matrix elements, the gauge cancellations between the three contributions

[20] There can be no orbital angular momenta in the s-channel as the annihilation of the electron and positron occurs at a point.

[21] In the relativistic limit the W boson couples only to negative helicity electrons and positive helicity positrons.

give $M \to 0$ for all helicity states. This is demonstrated in equation 2.26 for the example of $\lambda_1 = \lambda_2 = 1$, $\sigma_1 = -1, \sigma_2 = 1$.

$$\begin{aligned} M_{\lambda_1=1,\lambda_2=1,\sigma_1=-1,\sigma_2=1} &= -e^2\beta\sin\theta \\ &\quad +e^2\beta\frac{\gamma^2 m_w^2}{\gamma^2 m_w^2 - m_z^2}\left(1 - \frac{1}{2\sin^2\theta_w}\right)\sin\theta \\ &\quad +\frac{e^2}{\beta}\frac{1}{2\sin^2\theta_w}\left(1 - \frac{1}{\gamma^2}\frac{1}{1+\beta^2-2\beta\cos\theta}\right)\sin\theta \\ &\overset{s\to\infty}{\longrightarrow} -e^2\cdot 1\cdot\sin\theta \\ &\quad +e^2\cdot 1\cdot 1\cdot\left(1 - \frac{1}{2\sin^2\theta_w}\right)\sin\theta \\ &\quad +e^2\cdot 1\cdot\frac{1}{2\sin^2\theta_w}\cdot 1\cdot\sin\theta \\ &\longrightarrow 0 \end{aligned} \tag{2.26}$$

## 2.4 Angular Distributions and Cross-sections

The differential cross-sections calculated from the helicity amplitudes of the previous section are shown in figure 2.2.

It can be seen that the dominant contribution to the total cross-section comes from the two helicity states with $|\lambda - \bar{\lambda}| = 2$. These states have two units of spin angular momentum[22] and can only be generated through the t-channel neutrino exchange diagram (sections 2.1.2 and 2.3) and are not themselves affected by changes to the TGC's.

The seven helicity amplitudes which can be generated through the s-channel (in addition to the t-channel) represent the same degrees of freedom as the seven parameters in the phenomenological Lagrangian of equation 2.7. Sensitivity to TGC's at LEP2 comes mainly from the interference terms between the dominant t-channel *background* and the smaller s-channel *signal*.

Figure 2.3 shows the $W^-$ cross-sections averaged over the $W^+$ degrees of freedom. The large asymmetry of the distribution in the $W^-$ production angle, $\theta$, is a direct consequence of the prevalence of the t-channel [23] which tends to favour scattering through small angles [24] This, combined with the fact that the t-channel only contributes when the electron is

[22] The projection of the *total* angular momentum onto the beam axis still has to be equal to one.

[23] The s-channel distribution alone (summed over all helicity states) would be symmetric about $\theta = \frac{\pi}{2}$.

[24] Scattering through large angles in the t-channel requires the exchange of a neutrino with high momentum but negligible energy. Such a neutrino is highly virtual (far from mass-shell) and its production is therefore suppressed. This is encoded into the expression for $M_\nu$ in chapter 2.3 by the '$1 + \beta^2 - 2\beta\cos\theta$' term which appears in the denominator.

itself in a negative helicity state, explains the dominance of the negative helicity state of the $W^-$ boson.

The shape of the angular distribution of any individual helicity amplitude is independent of the anomalous couplings, which only vary the relative strengths of the amplitudes. Table 2.4 shows these anomalous coupling prefactors.

| | | $\bar{\lambda}$ | | |
|---|---|---|---|---|
| | | -1 | 0 | +1 |
| $\lambda$ | -1 | $g_1^V + 2\lambda_V\gamma^2 + \frac{\imath}{\beta}\left(\tilde{\lambda}_V(2\gamma^2-1) - \tilde{\kappa}_V\right)$ | $\gamma\left(a_V - \beta g_5^V + \imath\left(\frac{\tilde{\lambda}_V - \tilde{\kappa}_V}{\beta} - g_4^V\right)\right)$ | 0 |
| | 0 | $-\gamma\left(a_V + \beta g_5^V + \imath\left(\frac{\tilde{\lambda}_V - \tilde{\kappa}_V}{\beta} + g_4^V\right)\right)$ | $g_V - 2\gamma^2\kappa_V$ | $-\gamma\left(a_V - \beta g_5^V + \imath\left(\frac{\tilde{\kappa}_V - \tilde{\lambda}_V}{\beta} + g_4^V\right)\right)$ |
| | +1 | 0 | $\gamma\left(a_V + \beta g_5^V + \imath\left(\frac{\tilde{\kappa}_V - \tilde{\lambda}_V}{\beta} - g_4^V\right)\right)$ | $g_1^V + 2\lambda_V\gamma^2 - \frac{\imath}{\beta}\left(\tilde{\lambda}_V(2\gamma^2-1) - \tilde{\kappa}_V\right)$ |

Table 2.4: The anomalous coupling dependence of the $W^+W^-$ helicity amplitudes, $M_V$, where $V = Z$ or $\gamma$. $\lambda$ and $\bar{\lambda}$ are the helicities of the $W^-$ and $W^+$ respectively and $a_V \equiv g_1^V + \kappa_V + \lambda_V$.

The total angular distribution is formed from a coherent sum over all the helicity amplitudes and thus its shape does depend on the anomalous couplings. The same argument applies to the distributions of the $W^-$ helicity states averaged over the $W^+$ helicity states. The influence of the couplings is indicated in table 2.5, which gives a crude measure of the relative sensitivity of the $W^-$ distribution to individual anomalous TGC's.

| Helicity | | $g_1^Z$ | $\kappa_\gamma$ | $\kappa_Z$ | $\lambda_\gamma$ | $\lambda_Z$ | $\tilde{\kappa_Z}$ | $\tilde{\lambda_Z}$ | $g_4^Z$ | $g_5^Z$ |
|---|---|---|---|---|---|---|---|---|---|---|
| All | 64.3 | 61.8 | 61.5 | 61.5 | 60.9 | 62.5 | 66.2 | 65.7 | 64.7 | 64.6 |
| -ve | 53.9 | 52.9 | 52.9 | 53.2 | 52.9 | 53.4 | 55.3 | 54.7 | 54.1 | 53.5 |
| +ve | 86.6 | 82.5 | 85.3 | 83.8 | 85.3 | 81.0 | 87.4 | 87.3 | 86.8 | 88.3 |
| 0 | 70.3 | 64.9 | 62.5 | 62.6 | 60.1 | 67.1 | 72.3 | 72.3 | 70.9 | 70.7 |

Table 2.5: Effect of increasing anomalous couplings by 0.5 upon the average $W^-$ production angle in degrees. The first column of values are those from the SM. The first row of values shows the average angle obtained when all $W^-$ helicity states are included in the calculation. The rows beneath show the average angle obtained for each helicity state individually.

In practice, all of the parameters must be fitted to the data simultaneously. This requires as much information as possible on the W production angle and its spin or helicity state. The process of obtaining this information is outlined in chapter 3.

The magnitude of the total cross-section is also affected by the anomalous couplings. It can be written (equation 2.27) as a sum of contributions from the terms in the phenomenological Lagrangian. As the Lagrangian, and hence the amplitudes, are linear in the anomalous couplings, the cross-section is quadratic in them.

$$\begin{aligned} \sigma &= \sum_{i,j} x_i x_j \sigma_{ij} \\ x_i &\in \left\{ \Delta g_1^Z, \Delta\kappa_\gamma, \Delta\kappa_Z, \Delta\lambda_\gamma, \Delta\lambda_Z, \Delta\tilde{\kappa}_Z, \Delta\tilde{\lambda}_Z, \Delta g_4^Z, \Delta g_5^Z, \Delta_{SM} \right\} \end{aligned} \tag{2.27}$$

Here $\Delta_{SM}$ is a dummy variable equal to one in the standard model.

The coefficients, $\sigma_{ij}$, can be represented by the (non-unique) matrix, $\boldsymbol{\sigma}$, given in equation 2.28. Since the total cross-section is obtained by integrating over all kinematic variables and summing over all helicity states, the components of $\boldsymbol{\sigma}$ are simply numbers.

$$\boldsymbol{\sigma} = \begin{array}{c} \begin{array}{cccccccccc} \Delta g_1^Z & \Delta\kappa_\gamma & \Delta\kappa_Z & \Delta\lambda_\gamma & \Delta\lambda_Z & \Delta\tilde{\kappa}_Z & \Delta\tilde{\lambda}_Z & \Delta g_4^Z & \Delta g_5^Z & \Delta_{SM} \end{array} \\ \left[ \begin{array}{cccccccccc} .025 & .003 & .041 & .004 & .072 & .000 & .000 & .000 & .000 & -.001 \\ .000 & .014 & .004 & .038 & .002 & .000 & .000 & .000 & .000 & -.015 \\ .000 & .000 & .029 & .006 & .031 & .000 & .000 & .000 & .000 & -.004 \\ .000 & .000 & .000 & .028 & .002 & .000 & .000 & .000 & .000 & -0.20 \\ .000 & .000 & .000 & .000 & .072 & .000 & .000 & .000 & .000 & .003 \\ .000 & .000 & .000 & .000 & .000 & .082 & -.130 & .000 & .000 & .000 \\ .000 & .000 & .000 & .000 & .000 & .000 & .056 & .000 & .000 & .000 \\ .000 & .000 & .000 & .000 & .000 & .000 & .000 & .015 & .000 & .000 \\ .000 & .000 & .000 & .000 & .000 & .000 & .000 & .000 & .004 & -.002 \\ .000 & .000 & .000 & .000 & .000 & .000 & .000 & .000 & .000 & .300 \end{array} \right] \end{array} \begin{array}{c} \\ \Delta g_1^Z \\ \Delta\kappa_\gamma \\ \Delta\kappa_Z \\ \Delta\lambda_\gamma \\ \Delta\lambda_Z \\ \Delta\tilde{\kappa}_Z \\ \Delta\tilde{\lambda}_Z \\ \Delta g_4^Z \\ \Delta g_5^Z \\ \Delta_{SM} \end{array} \tag{2.28}$$

The matrix has been normalised by the arbitrary constraint in equation 2.29.

$$\sum_{i,j} \mid \sigma_{ij} \mid \; = \; 1 \tag{2.29}$$

The values in the array were calculated assuming a semi-leptonic tau decay mode for the W bosons (chapter 3) and including contributions from the left-handed helicity state of the tau only. Values for other decay modes will be similar.

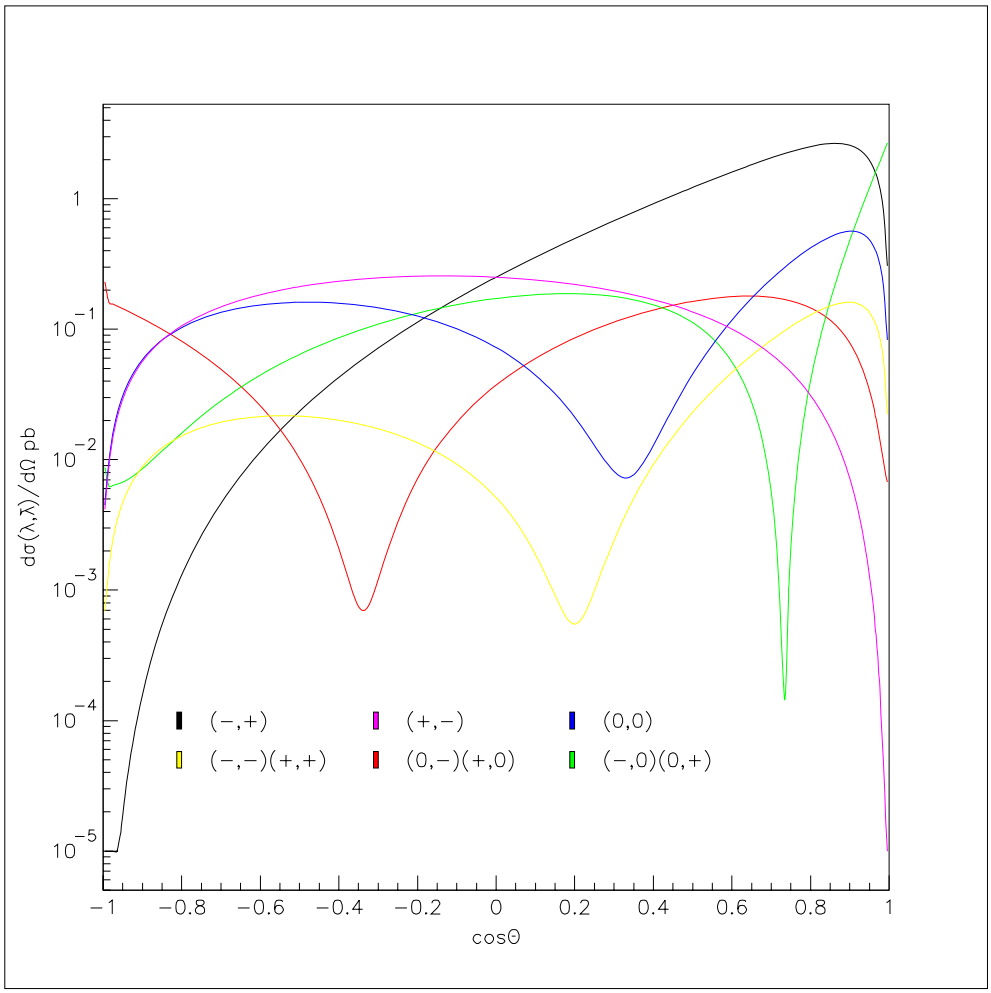


Figure 2.2: SM prediction of differential $W^+W^-$ production cross-section for specific helicity states at 189 GeV as a function of the cosine of the $W^-$ production angle with respect to the $e^-$ beam direction. $\lambda$ and $\bar{\lambda}$ are the $W^-$ and $W^+$ helicities respectively.

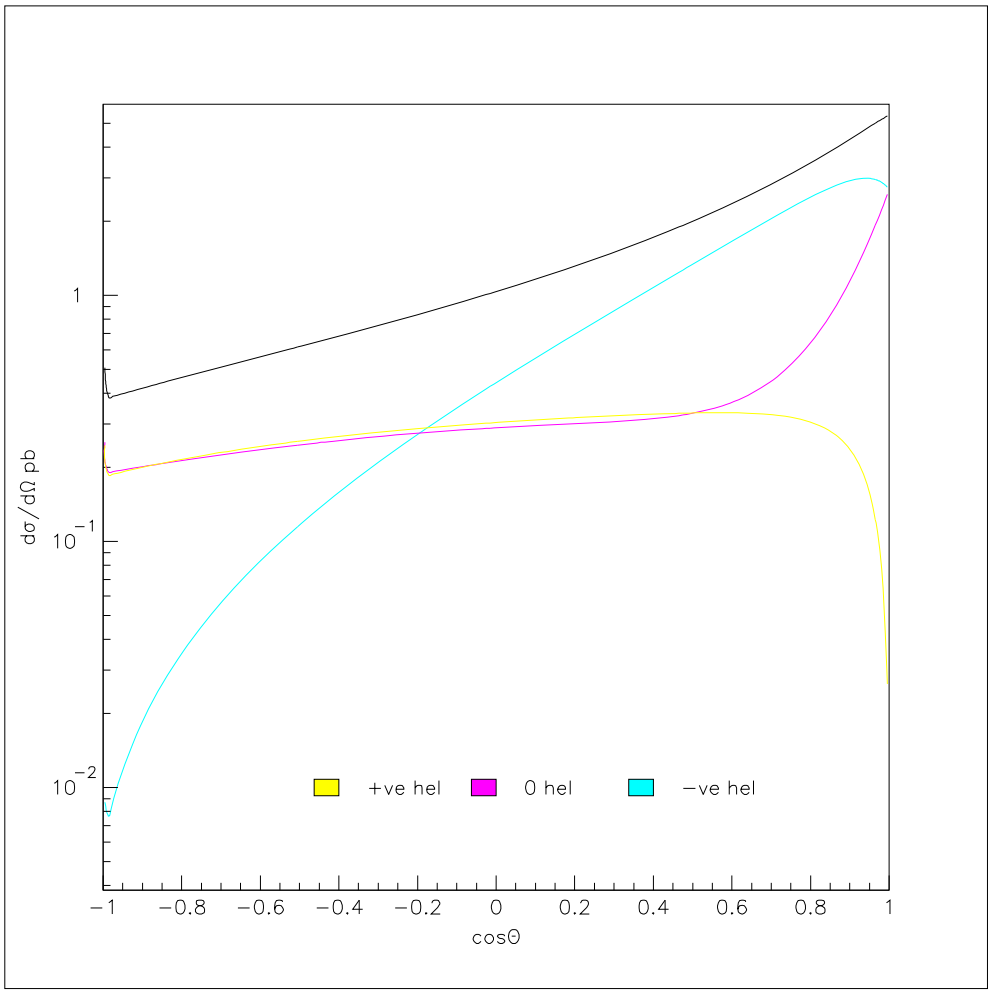


Figure 2.3: SM prediction of differential $W^-$ production cross-section for specific helicity states at 189 GeV as a function of the cosine of the $W^-$ production angle with respect to the $e^-$ beam direction. The black line shows the sum of the three helicity states.

# Chapter 3

# $W^+W^- \to q\bar{q}\tau\nu_\tau$ Decay

A W boson can decay either leptonically or hadronically. In either case the decay distributions depend on the direction of the spin vector of the *parent* W boson. Equivalently, the distributions depend on the relative proportion of the helicity states in the W boson's wavefunction. In this paper I consider a specific semi-leptonic decay for $W^+W^-$ events, in which one W decays to two quarks and the other to a tau and tau neutrino. This channel has a branching ratio of approximately 15%.

The hadronic decay cannot be treated using the perturbative method as the strong (colour field) interaction between quarks increases monotonically as a function of the quark separation. As the original quarks are separated, further quark anti-quark pairs are produced in a process known as hadronisation. This results in the formation of hadronic jets from which we can attemp to reconstruct the direction of the original W boson.

The neutrino produced in the leptonic decay is not expected to be detected, as it has a low interaction cross-section with conventional matter. This leaves the charged lepton as the only available source of information on the helicity of the W boson. In the case of the tau leptonic decay the tau is itself unlikely to be observed as it has a mean decay length of less than $4mm$ at LEP2 energies [7]. This is outside the instrumented volume of the OPAL detector (i.e. within the beam pipe)[1].

Therefore, the W and tau production angles have to be reconstructed from measurements of the energies and directions of the hadronic and tau jets. A method for partially recovering the tau angle for the case where the tau jet consists of a single pion is given towards the end of this chapter.

For reference, the general kinematics of a $q\bar{q}\tau\nu_\tau$ event are shown in figure 3.1.

[1]The inner radius of the silicon microvertex detector is 53.5mm.

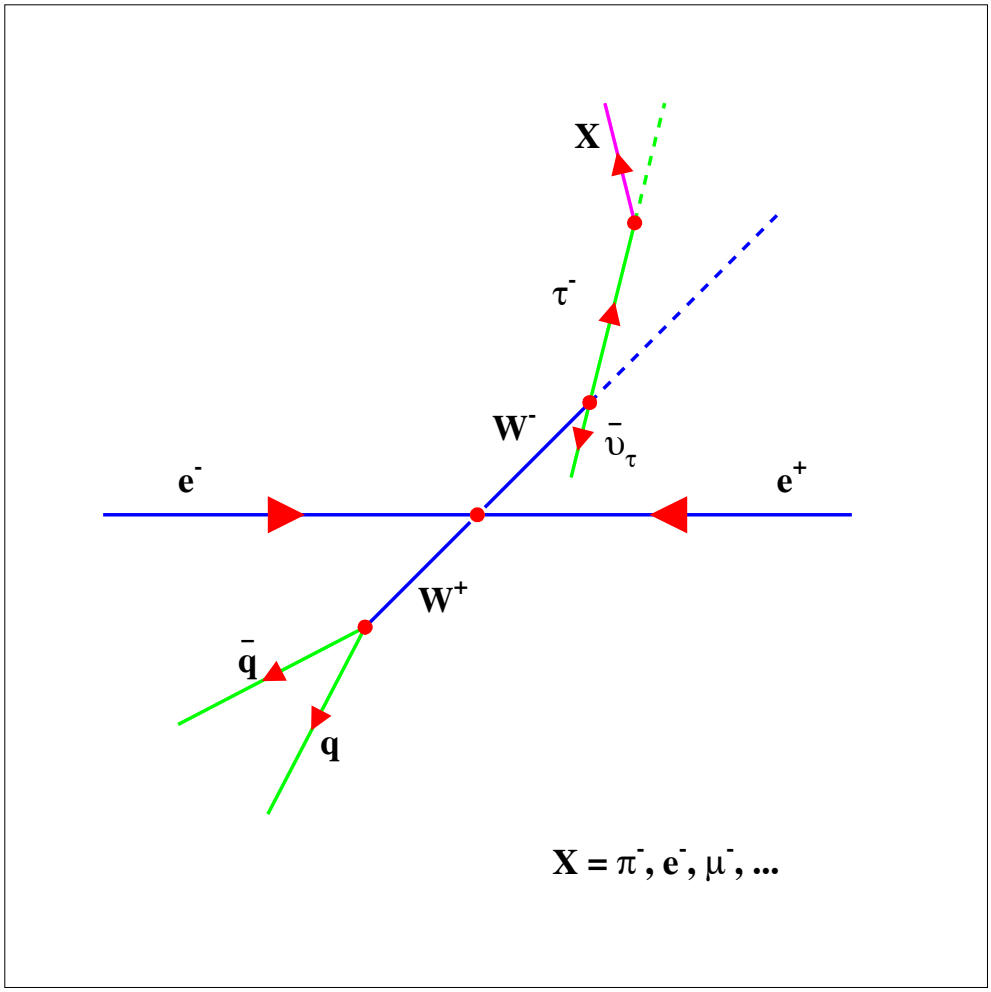


Figure 3.1: Kinematics of a generic $W^+W^- \to q\bar{q}\tau^-\bar{\nu}_\tau$ event, where X represents the observable decay products of the $\tau$.

Figures 3.2, 3.3 and 3.4 show first-order, standard model predictions of the relative differential cross-section for $e^+e^- \to W^+W^- \to q\bar{q}\tau^-\bar{\nu}_\tau$ events at 189 GeV as a function of the $W^-$ and $\tau^-$ production angles. These plots were generated in the mathematical analysis package 'Maple' using the density matrix formalism of Appendix A. The polar tau production angle, $\theta_\tau$, is calculated with respect to the $W^-$ direction. The azimuthal tau production angle, $\phi_\tau$, is calculated with respect to the plane defined by the $e^-$ beam direction and the $W^-$ direction. Strictly, the y-axis of this co-ordinate system is defined by the cross-product of these two directions in the order stated. [2]

The scale used for the vertical axis in the figures is arbitrary but consistent. It can readily be seen that the production of positive helicity taus is heavily suppressed compared to the production of negative helicity taus. This is a consequence of the V-A (vector minus axial-vector) form of the coupling between the W boson and the $\tau$ lepton.

Figure 3.2 shows that the majority of $W^-$ bosons and $\tau^-$ leptons are produced close to the $e^-$ beam direction. The behaviour of the $W^-$ boson has already been explained in section 2.4 as a consequence of the t-channel contribution to the amplitudes. The shape of the $\tau^-$ distribution can be understood from noting that both the $\tau^-$ and $W^-$ are preferentially produced in the negative helicity state. Angular momentum conservation then requires that the $\tau^-$ be emitted along the $W^-$ direction of motion (i.e. in the opposite direction to the $W^-$ spin vector).

Both the s-channel and t-channel have an azimuthal dependence in $\phi_\tau$ and the definition given above ensures that the differential cross-section is symmetric about $\phi_\tau = 0, \pi$. However, the exact form shown in figures 3.3 and 3.4 comes from the complicated interference between the two channels.

Details of the effects of anomalous couplings upon these distributions are given in Appendix B.

[2] Both the polar and azimuthal production angles of the tau lepton are *boosted* to the $W^-$ rest frame.

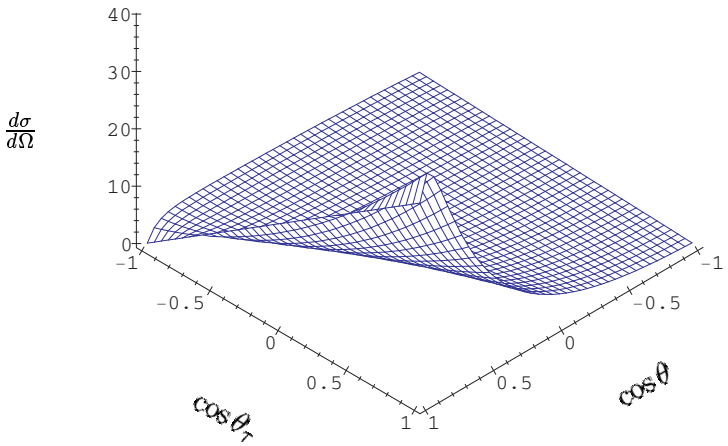


Negative helicity tau leptons.

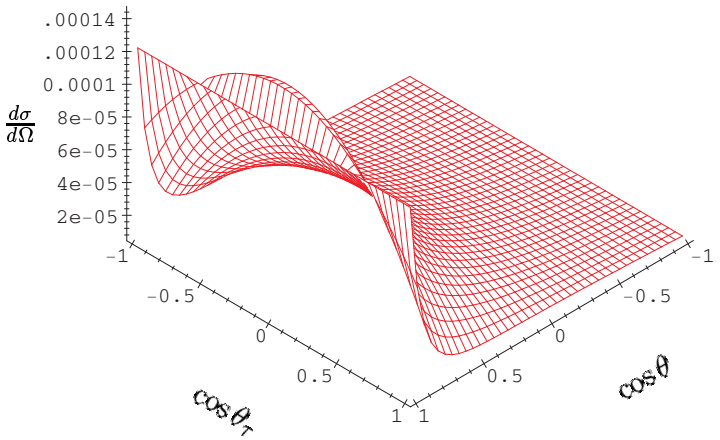


Positive helicity tau leptons.

Figure 3.2: Relative differential cross-section for $e^+e^- \to W^+W^- \to q\bar{q}\tau^-\bar{\nu}_\tau$ as a function of $\cos\theta$ and $\cos\theta_\tau$, where $\theta$ is the $W^-$ production angle and $\theta_\tau$ is the polar $\tau$ production angle boosted to the $W^-$ rest frame.

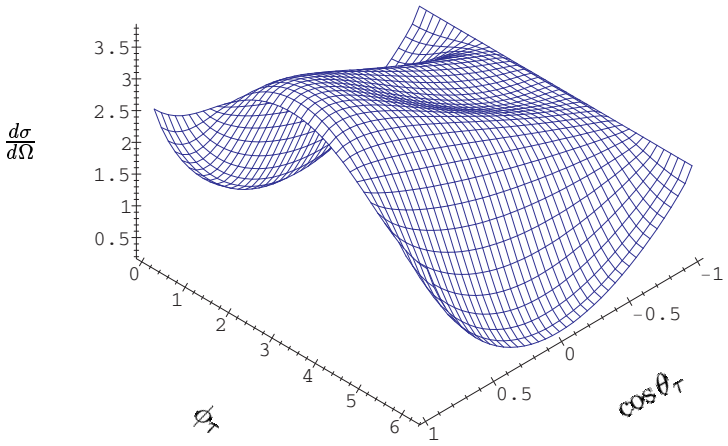


Negative helicity tau leptons.

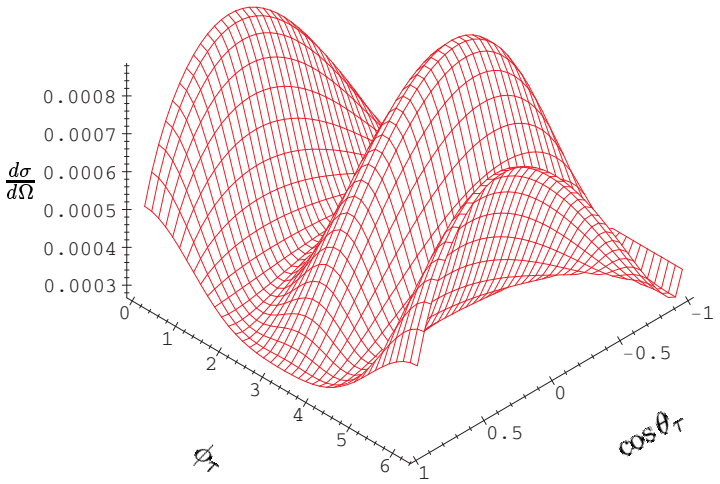


Positive helicity tau leptons.

Figure 3.3: Relative differential cross-section for $e^+e^- \to W^+W^- \to q\bar{q}\tau^-\bar{\nu}_\tau$ as a function of $\cos\theta_\tau$ and $\phi_\tau$, where $\theta_\tau$ and $\phi_\tau$ are the polar and azimuthal $\tau$ production angles boosted to the $W^-$ rest frame.

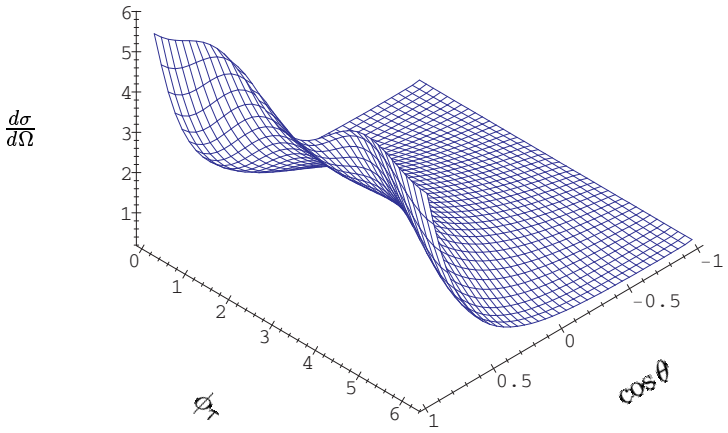


Negative helicity tau leptons.

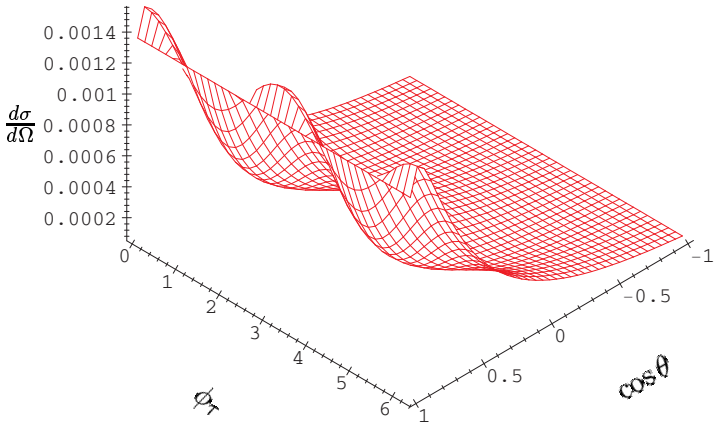


Positive helicity tau leptons.

Figure 3.4: Relative differential cross-section for $e^+e^- \to W^+W^- \to q\bar{q}\tau^-\bar{\nu}_\tau$ as a function of $\cos\theta$ and $\phi_\tau$, where $\theta$ is the $W^-$ production angle and $\phi_\tau$ is the azimuthal $\tau$ production angle boosted to the $W^-$ rest frame.

Approximately 10% of tau leptons decay to a tau neutrino, $\nu_\tau$, and a pion, $\pi$. The theoretical treatment of this decay mode is particularly simple as it is a two-body decay with no intermediate resonances to consider.

It is usual to approximate the direction of the tau by the direction of the tau jet [1]. However, as the pion mass ($m_\pi = 0.14GeV$) is only 8% of the tau mass, it is highly boosted in the tau rest-frame[3]. As it is also a scalar particle, its angular distribution is expected to show high sensitivity to the tau polarisation[4].

Therefore, the angle between the pion direction and the original tau direction in the lab frame, $\theta_{\tau\pi}$, cannot always be treated as negligible. The mean, standard deviation and maximum values for $\theta_{\tau\pi}$ at 189 GeV are: $\bar{\theta}_{\tau\pi} = 3.8^\circ, \sigma_{\tau\pi} = 0.9^\circ$ and $\theta_{\tau\pi}^{max} = 28^\circ$. Fortunately, this angle is strongly correlated with the energy of the pion in the lab frame, $E_\pi$. An analytical expression for this relationship has been evaluated and the result is plotted in figure 3.5.

In addition to knowing the magnitude of the deviation between the tau and the pion, it is necessary to know in which direction the deviation took place. Equations 3.1 to 3.7 show how the angle between the tau lepton and W boson in the lab frame can be estimated from measurements of the pion and W boson paths[5] and the function, $f(E_\pi, \theta_\tau)$, shown in figure 3.5. $\vec{l}_x$ is the position vector in the lab frame for a point on the path of particle 'x', parameterised by a distance $\lambda_x$. $\vec{a}_x$ is an arbitrary point on the path and $\vec{\hat{d}}_x$ is the direction vector of unit length. The origin of the co-ordinate system is defined as the $W^+, W^-$ production point. It is assumed that the tau lepton path also begins at the origin since the mean distance travelled by each W boson before it decays is negligible (around $6 \times 10^{-17}$m at 189 GeV).

$$\vec{l}_\pi = \vec{a}_\pi + \lambda_\pi \vec{\hat{d}}_\pi \tag{3.1}$$

$$\vec{l}_w = \lambda_w \vec{\hat{d}}_w \tag{3.2}$$

$$\vec{l}_\tau = \lambda_\tau \vec{\hat{d}}_\tau \tag{3.3}$$

The paths of the pion and tau are constrained (equation 3.4) to cross at some point parameterised by a distance, $\lambda'_\pi$, along the pion path (from point $\vec{a}_\pi$) and a distance, $\lambda'_\tau$, along the tau path (from the origin).

[3]The velocity of the tau in the W rest frame is approximately $0.999c$. The velocity of the pion in the tau rest frame is approximately $0.988c$.

[4]The transition rate for the single pion decay of a negative helicity tau is proportional to $(1 - \cos\theta_\pi)$, where $\theta_\pi$ is defined with respect to the direction of motion of the tau. I.e. Most pions are emitted 'backwards' in the tau rest frame.

[5]The W boson path is reconstructed from the hadronically decaying W.

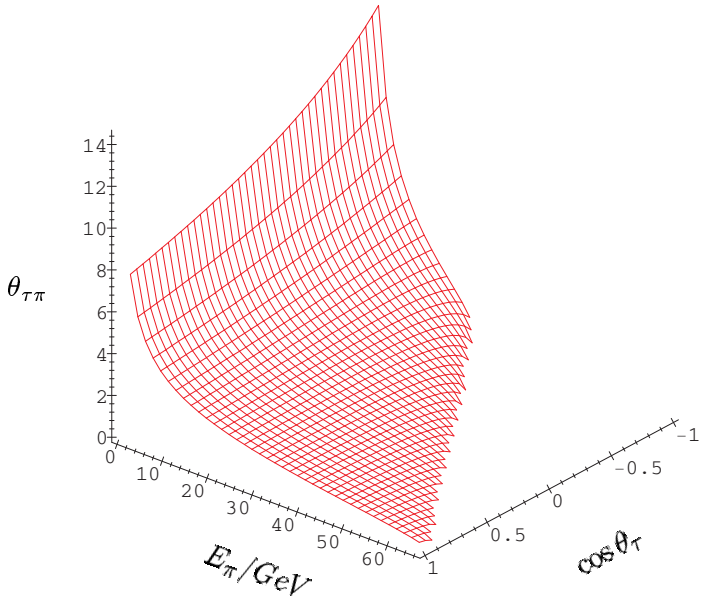


Figure 3.5: Angle between $\tau$ and $\pi$ in the lab frame as a function of the energy of the pion, $E_\pi$, and the tau production angle $\theta_\tau$ . The peak at low energy for tau leptons travelling backwards with respect to the W boson direction is resolution limited in this plot.

$$\vec{l}_\pi(\lambda'_\pi) = \vec{l}_\tau(\lambda'_\tau) \tag{3.4}$$

Substituting equations 3.1 and 3.3 into equation 3.4 and then taking the scalar product with the pion and W direction vectors gives equations 3.5 and 3.6.

$$\Rightarrow \lambda'_\tau(\vec{\hat{d}}_\tau \cdot \vec{\hat{d}}_\pi) = \vec{a}_\pi \cdot \vec{\hat{d}}_\pi + \lambda'_\pi \tag{3.5}$$

$$\lambda'_\tau(\vec{\hat{d}}_\tau \cdot \vec{\hat{d}}_w) = \vec{a}_\pi \cdot \vec{\hat{d}}_w + \lambda'_\pi(\vec{\hat{d}}_\pi \cdot \vec{\hat{d}}_w) \tag{3.6}$$

Eliminating $\lambda'_\pi$ and rewriting some of the scalar products in terms of cosines gives equation 3.7.

$$\Rightarrow \cos\theta^{LAB}_{\tau w} = \frac{\vec{a}_\pi \cdot \vec{\hat{d}}_w + (\lambda'_\tau \cos\theta^{LAB}_{\tau\pi} - \vec{a}_\pi \cdot \vec{\hat{d}}_\pi)\cos\theta^{LAB}_{\pi w}}{\lambda'_\tau} \tag{3.7}$$

$$\theta^{LAB}_{\tau\pi} = f(E_\pi, \theta_\tau) \tag{3.8}$$

$$\approx f(E_\pi, \theta_\pi) \tag{3.9}$$

$\lambda'_\tau$ is the distance travelled by the tau lepton before it decays to the pion, as given by equation 3.10.

$$\lambda'_\tau = \frac{|\vec{a}_\pi \times \vec{\hat{d}}_\pi|}{\sin\theta^{LAB}_{\tau\pi}} \tag{3.10}$$

Figure 3.6 compares those values obtained for the angle between the tau lepton and W boson in the lab frame using equation 3.7 with those obtained from the assumption that the pion and tau directions are identical. The former method shows a large improvement over the simpler approach (the standard deviation is reduced to $0.61^\circ$ from $3.65^\circ$). It is hoped that further work in this area will give better reconstruction of the tau direction for all the tau decay channels and hence increase the sensitivity to anomalous TGC's.

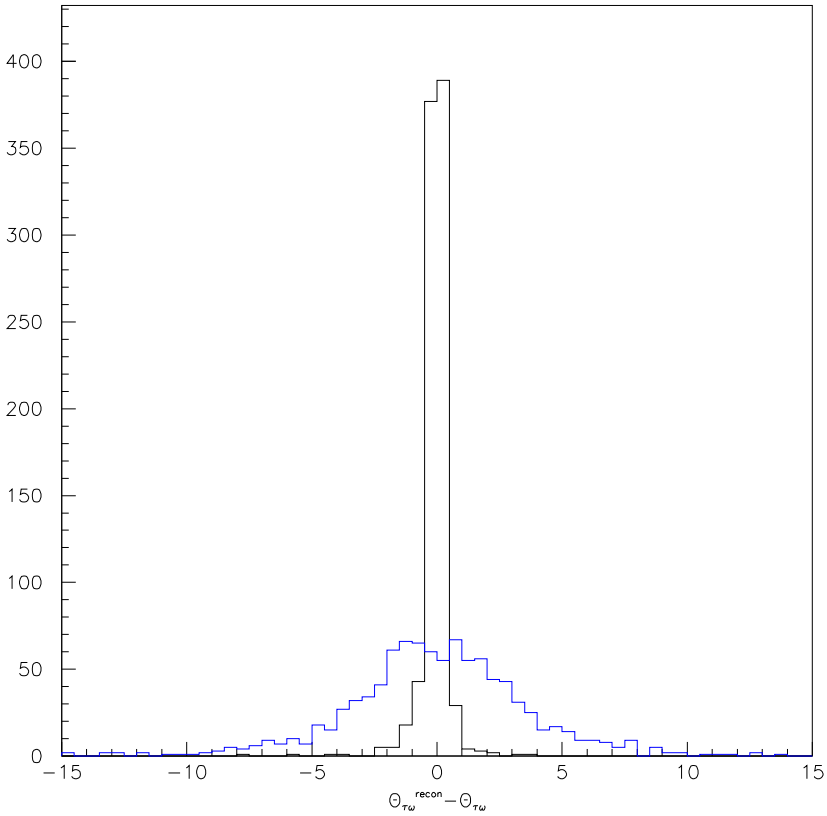


Figure 3.6: Histogram of Monte Carlo $e^+e^- \to W^+W^- \to q\bar{q}\tau\nu_\tau \to \pi\nu_\tau$ events generated using KoralW1.33 (run 7323) showing the angle between the tau lepton and W boson in the lab frame subtracted from the reconstructed angle. The black histogram was generated using equation 3.7 and the blue histogram from approximating the tau direction by the pion direction.

# Chapter 4

# Conclusions

This paper has reviewed the concept and properties of anomalous triple gauge boson couplings and their parameterisation in the Lagrangian for $W^+W^-$ production at LEP2.

Tree-level standard model predictions of the distributions for $W^-W^+$ production and subsequent semi-leptonic decay to a tau lepton have been presented. The dependence of the distributions on the nine parameters commonly used in the literature to describe the most general possible $\gamma WW$ / $ZWW$ vertex has been explored and analytical expressions calculated.

Finally, in order to enhance the sensitivity of the analysis of LEP2 data to anomalous TGC's, an improved method for extracting the angle of the tau from the angle of its decay products has been introduced.

It's hoped that this paper will prove to be a useful reference for future investigations of the $q\bar{q}\tau\nu_\tau$ channel, as much work remains in improving the reconstruction of these events. At present, neither the method for recovering the W boson direction (not presented here) nor that for recovering the $\tau$ direction appear to be optimal. Other questions that have not yet been addressed include:

- Whether the small positive helicity tau contribution may carry valuable, measurable and as yet un-modelled information on anomalous TGC's.
- Whether the hadronic jets can be used to recover helicity information for the hadronically decaying W boson.
- Whether an optimal observables method [7] can be developed for this decay channel.
- What applications the kinematic analysis used to to generate the results in this paper may have in the process of discriminating $q\bar{q}\tau\nu_\tau$ from other channels.

# Bibliography


[1] OPAL Collaboration, OPAL Physics Note PN354 (1998)

[2] Caso, C. et al, Particle Data Group, European Physical Journal C **3** (1998) 1 l

[3] G. Altarelli, T. Sjöstrand, F. Zwirner, CERN **96-01** (1996)

[4] CDF Collaboration, F. Abe et al, Phys. Rev. Lett. **75** (1995) 1034

[5] G.J. Gounaris, F.M. Renard, G. Tsirigoti, Phys. Lett. B **350** (1995) 212

[6] G.J. Gounaris, F.M. Renard, G. Tsirigoti, Phys. Lett. B **338** (1994) 51

[7] M. Diehl, O. Nachtmann, Z. Phys C **62** (1994) 397

[8] G.J. Gounaris, F.M. Renard , Z. Phys C **59** (1993) 131

[9] M. Bilenky, J.L. Kneur, F.M.Renard, D. Schildknecht, Nucl. Phys. B **409** (1993) 22

[10] J.M. Frère, M. Tytgat, J.M. Moreno, J. Orloff, Nucl Phys. B **429** (1994) 3

[11] G. Altarelli, CERN-TH 6305-91 (1991)

[12] M.S. Chanowitz, Ann. Rev. Nucl. Part Sci. **38** (1988) 323

[13] K. Hagiwara, R.D. Peccei, D. Zeppenfeld, K. Hikasa, Nucl. Phys B **282** (1987) 253

[14] W. Buchmüller, D. Wyler, Nucl. Phys B **268** (1986) 621

[15] C.N. Leung, S.T. Love, S. Rao, Z. Phys C **31** (1986) 433

[16] K.J.F. Gaemers, G.J. Gounaris, Z. Phys C **1** (1979) 259

[17] M.L. Perl, High Energy Hadron Physics, Wiley (1974) 256

# Chapter 5

# Appendix A: The Density Matrix

The density matrix describes physical states which are both statistical and quantum mechanical in nature. The wavefunction of a pure quantum mechanical system, $\Psi$, can be expressed as a coherent sum over a complete set of accessible eigenstates, $\phi_i$, as in equation 5.1.

$$\Psi = \sum_{i=1}^{n} a_i \phi_i \tag{5.1}$$

The expectation value of some observable, $O$, is shown in equation 5.2.

$$< O > = \sum_{i=1}^{n} \sum_{j=1}^{n} a_i a_j < \phi_i | O | \phi_j > \tag{5.2}$$

A more general system may be in one of N different quantum mechanical states, $\Psi_k$, with some statistical probability, $p_k$. The expectation value for $O$ for such a system is shown in equation 5.3.

$$< O > = \sum_{k=1}^{N} \sum_{i=1}^{n} \sum_{j=1}^{n} a_{i,k} a_{j,k} p_k < \phi_i | O | \phi_j > \tag{5.3}$$

This situation can arise where we do not have complete knowledge of a system's history. In the case of $W^+W^-$ production at LEP2 the initial $e^+e^-$ polarisations for a particular event are unknown. The resulting W pair system is therefore in one of two possible pure quantum mechanical states [1].

[1] Although there are four possible polarisations for $e^+e^-$ only two of these can result in a W pair at tree level.

Equation 5.3 can be rewritten as in equation 5.4, where the entity, $\rho$, is the density matrix for the basis $\phi$, shown explicitly in equation 5.5.

$$< O > \quad = \quad \sum_{i=1}^{n} \sum_{j=1}^{n} \rho_{ij} < \phi_i | O | \phi_j > \tag{5.4}$$

$$\rho_{ij} \quad = \quad \sum_{k=1}^{N} a_{i,k} a_{j,k} p_k \tag{5.5}$$

Calculations carried out in this paper use the density matrix with a basis of helicity eigenstates. The $W^+W^-$ density matrix is found using equation 5.6 which relates it to the $e^+e^-$ density matrix through the helicity amplitudes, M, of section 2.3. Assuming that the electrons and positrons are unpolarised, their density matrix, $\rho^{e^+e^-}_{\sigma_1,\sigma_2;\sigma_1',\sigma_2'}$, is just the $4 \times 4$ identity matrix and equation 5.6 reduces to equation 5.7.

$$\rho^{W^+W^-}_{\lambda_1,\lambda_2;\lambda_1',\lambda_2'} \quad = \quad \sum_{\sigma_1,\sigma_2;\sigma_1',\sigma_2'} M(\lambda_1,\lambda_2,\sigma_1,\sigma_2) \cdot M^*(\lambda_1',\lambda_2',\sigma_1',\sigma_2') \cdot \rho^{e^+e^-}_{\sigma_1,\sigma_2;\sigma_1',\sigma_2'} \tag{5.6}$$

$$= \quad \sum_{\sigma_1,\sigma_2} M(\lambda_1,\lambda_2,\sigma_1,\sigma_2) \cdot M^*(\lambda_1',\lambda_2',\sigma_1,\sigma_2) \tag{5.7}$$

The differential cross-section for a specific helicity state is just given by the appropriate diagonal element from the $W^+W^-$ density matrix, as shown in equation 5.8. The constant of proportionality is the reciprocal of the trace of the $e^+e^-$ density matrix (i.e. in this case simply $\frac{1}{4}$).

$$\left( \frac{d\sigma^{W^+W^-}}{d\Omega} \right)_{\lambda_1,\lambda_2} \quad \propto \quad \rho^{W^+W^-}_{\lambda_1,\lambda_2;\lambda_1,\lambda_2} \tag{5.8}$$

The tau lepton density matrix is generated in an entirely analogous way; the general form of equation 5.6 is used to relate the tau matrix to the $W^+W^-$ matrix through the tau production helicity amplitudes.

# Chapter 6

# Appendix B: Anomalous Contributions to the $q\bar{q}\tau\nu_\tau$ Differential Cross-Section

Following the convention of equations 2.27 and 2.28 the differential cross-section for $e^+e^- \rightarrow W^+W^- \rightarrow q\bar{q}\tau^-\bar{\nu}_\tau$ events can be written as a sum of contributions from the terms of the phenomenological Lagrangian. This is shown explicitly in equation 6.1 where $\Omega$ is taken to be $(\phi_\tau \cdot \cos\theta_\tau \cdot \cos\theta)$.

$$\begin{aligned} \frac{d\sigma}{d\Omega} &= \sum_{i,j} x_i x_j \, \partial\sigma_{ij} \\ x_i &\in \left\{\Delta g_1^Z, \Delta\kappa_\gamma, \Delta\kappa_Z, \Delta\lambda_\gamma, \Delta\lambda_Z, \Delta\tilde{\kappa}_Z, \Delta\tilde{\lambda}_Z, \Delta g_4^Z, \Delta g_5^Z, \Delta_{SM}\right\} \end{aligned} \tag{6.1}$$

Setting $\Delta_{SM}$ to one and assuming that terms which are second order in the anomalous couplings are small reduces equation 6.1 to equation 6.2.

$$\frac{d\sigma}{d\Omega} = \sum_i x_i \, \partial\sigma_i \tag{6.2}$$

Once the $\phi_\tau$ and $W^+$ [1] dependence has been integrated out the $\partial\sigma_i$ can be written as a finite power series in the cosines of the $W^-$ and $\tau^-$ production angles as in equation 6.3, where 'n' runs between zero and four inclusive and 'm' runs between zero and two inclusive.

$$\partial\sigma_i \times (b_1 - b_2\cos\theta) = \sum_{nm}^{NM} a_{nm}^{(i)} \times \cos^n\theta \times \cos^m\theta_\tau \tag{6.3}$$

[1] For this calculation the $W^+$ boson is always assumed to decay hadronically.

This summation on the right-hand side is related trivially to a two dimensional Fourier transform.

The values of the coefficients, $a_{nm}^{(i)}$ calculated at 189 GeV from the tree-level Feynman diagrams are shown in table 6.1 [2]. At this energy $b_1$ and $b_2$ take the values 1.28 and 1.05 respectively. The expression for $\partial\sigma$ associated with $\Delta_{SM}$ has been multiplied by an extra factor of $(b_1 - b_2 \cos\theta)$ to give it the same form as the other expressions.

| $n, m$ | 0,0 | 0,1 | 0,2 | 1,0 | 1,1 | 1,2 | 2,0 |
|---|---|---|---|---|---|---|---|
| $\Delta g_1^Z$ | -.080 | -.146 | .012 | .167 | -.138 | -.010 | .002 |
| $\Delta\kappa_\gamma$ | -.130 | -.091 | .085 | .210 | -.044 | -.212 | .040 |
| $\Delta\kappa_Z$ | -.113 | -.146 | .074 | .258 | -.138 | -.289 | .034 |
| $\Delta\lambda_\gamma$ | -.195 | -.091 | .150 | .372 | -.044 | -.375 | .105 |
| $\Delta\lambda_Z$ | -.078 | -.146 | -.039 | .229 | -.138 | .260 | .000 |
| $\Delta\tilde{\kappa_Z}$ | .000 | .000 | .000 | .000 | .000 | .000 | .000 |
| $\Delta\tilde{\lambda_Z}$ | .000 | .000 | .000 | .000 | .000 | .000 | .000 |
| $\Delta g_4^Z$ | .000 | .000 | .000 | .000 | .000 | .000 | .000 |
| $\Delta g_5^Z$ | -.077 | -.021 | .000 | -.073 | -.016 | .000 | .223 |
| $\Delta_{SM}$ | .766 | .206 | .337 | -.363 | 1.119 | .239 | -.205 |

| $n, m$ | 2,1 | 2,2 | 3,0 | 3,1 | 3,2 | 4,0 | 4,2 |
|---|---|---|---|---|---|---|---|
| $\Delta g_1^Z$ | .424 | -.012 | .062 | .000 | .010 | .000 | .000 |
| $\Delta\kappa_\gamma$ | .230 | -.085 | -.033 | .000 | .212 | .000 | .000 |
| $\Delta\kappa_Z$ | .424 | -.074 | -.029 | .000 | .289 | .000 | .000 |
| $\Delta\lambda_\gamma$ | .230 | -.150 | -.196 | .000 | .375 | .000 | .000 |
| $\Delta\lambda_Z$ | .424 | .039 | .000 | .000 | -.260 | .000 | .000 |
| $\Delta\tilde{\kappa_Z}$ | .000 | .000 | .000 | .000 | .000 | .000 | .000 |
| $\Delta\tilde{\lambda_Z}$ | .000 | .000 | .000 | .000 | .000 | .000 | .000 |
| $\Delta g_4^Z$ | .000 | .000 | .000 | .000 | .000 | .000 | .000 |
| $\Delta g_5^Z$ | -.021 | .000 | .000 | .137 | .000 | .000 | .000 |
| $\Delta_{SM}$ | .552 | -.241 | -.012 | -.637 | -.239 | -.049 | -.096 |

Table 6.1: The coefficients, $a_{nm}$, from the expansion of the differential cross-section in terms of the anomalous couplings and the cosines of the $W^-$ and $\tau^-$ production angles at 189 GeV. Only the left-handed helicity state of the tau leptons has been considered.

[2] Note that $a_{4,1}$ is always zero.

The contour plots in figure 6.1 show the distributions associated with each anomalous coupling, except for $\tilde{\kappa_Z}, \tilde{\lambda_Z}$ and $g_4^Z$ which give no contribution. The plots are of the ratio of the anomalous distributions to the standard model distribution. The hyperbolic tangent has been taken to prevent the sharp peaks that typically occur near $\cos\theta = \cos\theta_\tau = \pm 1$ from obscuring more subtle features.

Although the behaviour is complicated it can be seen that $\Delta\kappa_\gamma$ and $\Delta\kappa_Z$ tend to interfere destructively, such that a positive deviation of one will tend to hide a positive deviation of the other. The same is true of $\Delta\lambda_\gamma$ and $\Delta\lambda_Z$.

The three couplings which do not give contributions are CP violating (see table 2.3). Their presence is *only* discernible from the $\phi_\tau$ distribution. The relevant contour plots are shown in figure 6.2 and can be seen to be anti-symmetric about $\phi_\tau = \pi$. (The hyperbolic tangent is not taken for these plots.)

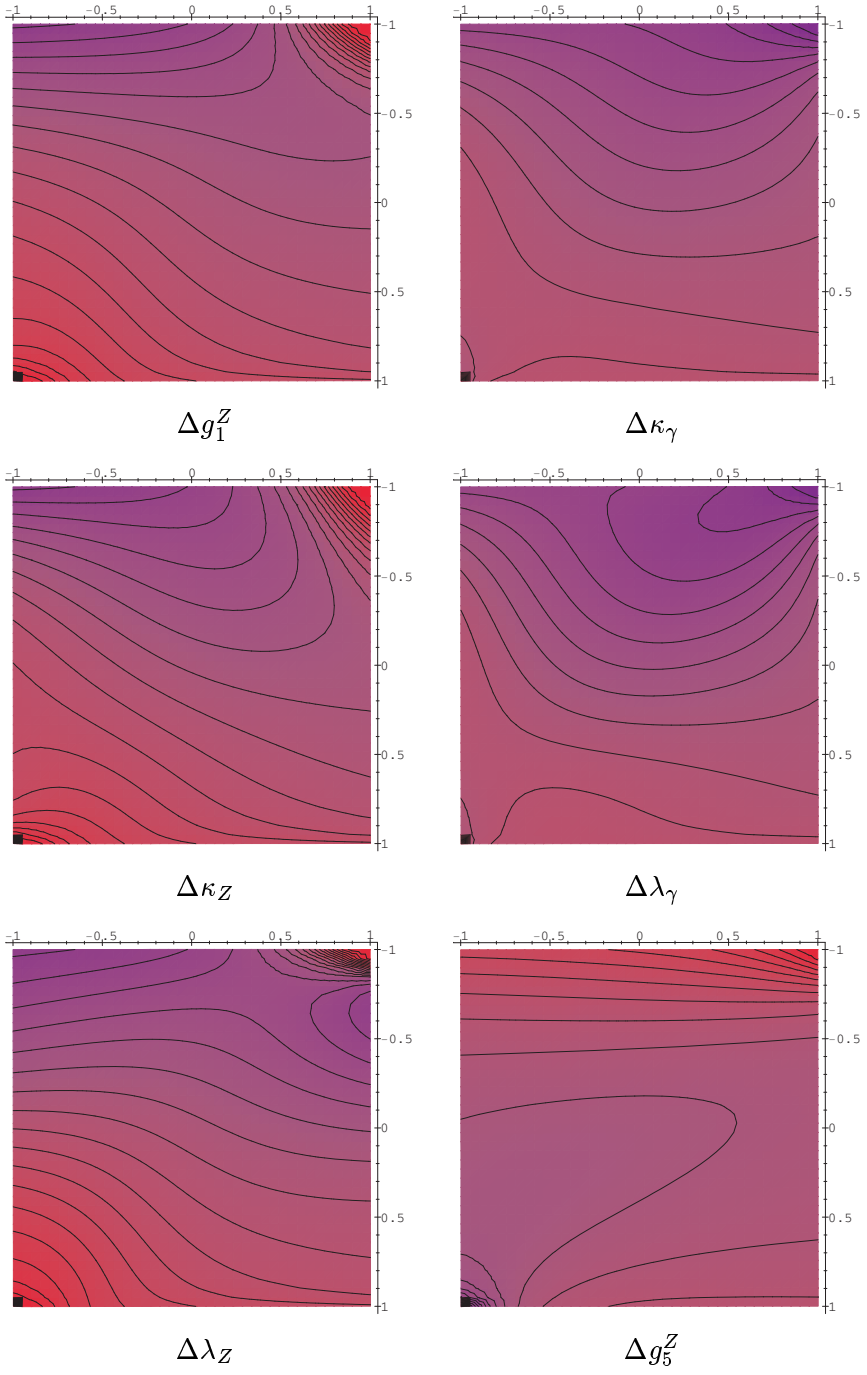


Figure 6.1: Contour plots of the hyperbolic tangent of the ratio $\partial\sigma^i/\partial\sigma^{\Delta_{SM}}$. $\cos\theta$ runs vertically and $\cos\theta_\tau$ runs horizontally. Positive values are shaded red, negative values are shaded blue.

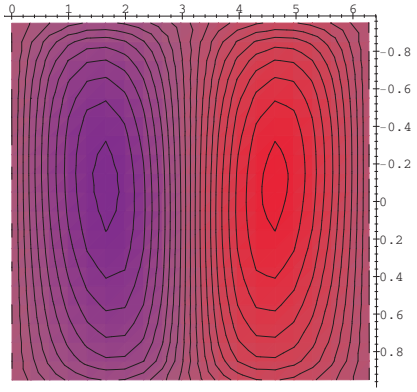


$\Delta\tilde{\kappa_Z}$

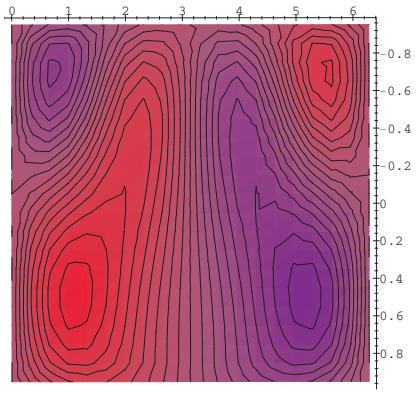


$\Delta\tilde{\lambda}_Z$

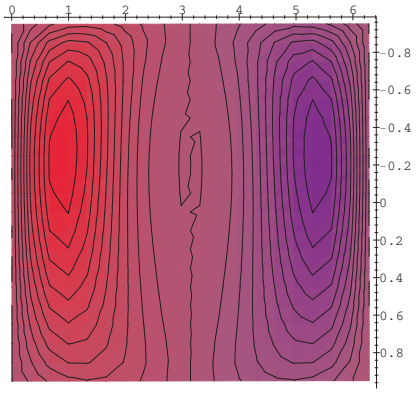


$\Delta g_4^Z$

Figure 6.2: Contour plots of the ratio $\partial\sigma^i/\partial\sigma^{\Delta_{SM}}$. $\cos\theta$ runs vertically and $\phi_\tau$ runs horizontally. Positive values are shaded red, negative values are shaded blue.